Duty Cycle Modulation and Fuzzy Controller of a Chopper Extracting the Maximum Power Point of a Solar Panel

Kengnou Donfack Clement*, Kom Charles Hubert‡,**, Moffo Lonla Bertrand*

*Laboratory of Computer Science Engineering and Automation, Higher Normal School of Technical Education of Douala, University of Douala, Po Box 2701 Douala, Cameroon

**Laboratory of Energy, Materials, Modelling and Methods, National Higher Polytechnic School of Douala, University of Douala, Po Box 2701 Douala, Cameroon

(kengnou@yahoo.fr,charleshubert.kom@gmail.com, moffolb@yahoo.fr)

‡Corresponding Author; Kom Charles Hubert, Po Box 2701 Douala, Cameroon, Tel:+237 696456745,

charleshubert.kom@gmail.com

Received: 05.12.2021 Accepted: 21.01.2022

Abstract-Photovoltaic (PV) solar energy is a renewable energy source that the world should exploit in abundance to increase its energy supply. However, its production is strongly influenced by sunshine and ambient temperature. Thus, its power-voltage characteristic is impacted by atmospheric conditions and thus hinders its operation at the point of maximum power. However, there are several algorithms in the literature, making it possible to extract at any time the maximum power from the PV, whose operating principle consists in modifying the duty cycle of a converter placed between the source (PV) and the load in order to operate the assembly at the point of maximum power.In this article, we propose a new strategy for finding the maximum power point (MPP), based on the fuzzy controller and the duty cycle modulator (DCM). This strategy (fuzzy-DCM) consists in positioning the DCM at the output of the fuzzy controller in order to control the DC-DC converter, placed between the PV and the load.The objectives of this strategy are, on the one hand, to improve the speed of convergence towards the MPP, and on the other hand, to reduce the oscillations around this point. This strategy is later tested on the Matlab/Simulink environment on a 250kW solar power plant and compared to the Fuzzy-PWM strategy. The test results show that the Fuzzy-DCM strategy improves the convergence speed by 2,013 times that of the Fuzzy-PWM strategy. In addition, it also reduces the oscillations around the MPP by 2.36 times lower than the Fuzzy-PWM strategy.Finally, we can say that the Fuzzy-DCM strategy is faster and more accurate than the Fuzzy-PWM strategy.

Keywords: MPPT, MPP, fuzzy controller, PWM, DCM, photovoltaic panel.

Nomenclature

DCM	Duty Cycle Modulation	MPPT	Maximum Power Point Tacking
PWM	Pulse With Modulation	OPAM	Operational Amplifier
MPP	Maximum Power Point	PV	Photovoltaic
DC	Direct Current	R	resistance
I	Current	L	Inductance
V	Voltage	C	Capacitor
N-DCM	Neuro Duty Cycle Modulator	NF-DCM	Neuro Fuzzy Duty Cycle Modulator
V_{opt}	Optimal Voltage	V_{OC}	Open Circuit Voltage
I_{opt}	Optimal Current	I_{SC}	Short Circuit Current

1. Introduction

The ever-increasing energy needs are pushing the world to find other sources of energy in order to increase its energy supply [1]. Among these new energy sources, we find photovoltaic solar energy, the production of which is impacted not only by sunlight, but also by ambient temperature. And its operating point depends on atmospheric conditions (sunshine and temperature) and the characteristics of the connected load [2]. Indeed, for a given load and precise atmospheric conditions, there is a single point of optimal operation, called point of maximum power (MPP). Thus, when the source and the load are connected directly to each other, the operating point of the assembly is rarely optimal. So, when these conditions change, we will operate more or less far from the point of maximum power,load to operate the assembly at the point of maximum power. This converter can be a step-up (Boost [3]), step-down (Buck [4]) or Buck-Boost chopper. By varying the duty cycle of the converter according to the variation in atmospheric conditions, we force the PV to operate at MPP [2].

Indeed, this problem of pursuit of maximum power is the subject of much research to this day. There are in the literature,

different types of algorithms for MPPT research such as MPPTs based on voltage or current regulation, conductance increment (IC), disturbance and observation (P&O) and logic blurred [5]. In this context, the MPPT technique based on voltage or current regulation, exploits the proportionality relationship between the optimal values of the maximum power point (V_{opt} and I_{opt}) and the no-load (open circuit) and short-circuit parameters (V_{OC}andI_{SC}) of the photovoltaic module. However, although this technique is easy to implement, but it is limited by low accuracy due to parameter estimation methods that require power transfer shutdown. And in addition, under variations in climatic conditions, this technique presents inefficiency in monitoring the MPP [5]-[6]. On the other hand, the search technique based on the IC, exploits the variation of the conductance of the GPV and its influence on the position of the operating point. This technique is very complex than techniques based on voltage or current regulation, and moreover, it has a long execution time, which reduces its convergence speed[5], [7]. As for the P&O algorithm which consists of causing a small disturbance on the voltage V and observing the evolution of the power in order to determine the MPP. Although this algorithm is simple and requires less measured parameters, however, it causes permanent oscillations around the MPP. To solve the problem of permanent oscillations around the MPP, some researchers [8]-[10] have proposed reducing the value of the increment step. However, a small increment value slows down the search for the MPP. For others [5], [11], the solution is to use the fuzzy controller which is well suited to this type of problem because of its speed of converging. In addition, fuzzy control, known for its robustness, is adaptive in nature, which gives it great performance in varying system parameters and disturbances.

However, at the output of the fuzzy controller, there is a modulator whose role is to convert the duty cycle emitted from this controller into pulses making it possible to control the chopper. The pulse width modulator (PWM) is widely used for that purpose [5]. However, the performance of the entire control is most of the time affected by the use of the PWM modulator. Therefore, it introduction in the chain of command not only lead to a problem of precision (following the setpoint), but also that of speed. However, the duty cyclic modulator (DCM) seems to be an alternative solution since it is known and has proven itself in several fields, in particular in power electronics [12]-[13], in signal transmission, in digital signal processing, etc.… Compared to PWM which operates at a fixed frequency, the operating frequency of the DCM is a function of the input signal that make his frequency spectrum poor in harmonics compare to that of PWM [1]. Which is an asset for the latter. And this operating principle can be favourable to us, in particular in the follow-up of the setpoint and the speed of convergence.

2. Methodology and Research Tools

Structure of our system, illustrated in Figure 1, shows that it consists essentially of a solar panel, a Boost chopper converter, a load and a Fuzzy-DCM command chain.

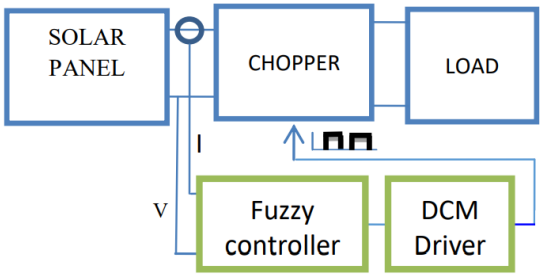

Fig. 1. Fuzzy-DCM MPPT command block diagram.

2.1. Modeling of the photovoltaic solar panel.

We will start with Modeling a photovoltaic cell.

2.1.1 Modeling of the photovoltaic cell

This modeling involves determining the cell voltage and current equations as a function of lighting and ambient temperature[2]. Figure 2 shows PV cell.

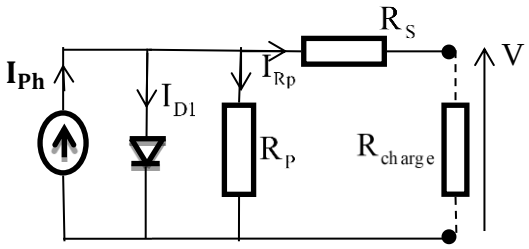

Fig.2. PV modeling scheme.

I_{ph}, I_{D1}, I_{RP} and I, Represent respectively, the photo current from the illuminance, the current in the diode, the current in the parallel resistor and the current in the load. At any time,

$$I = I_{Ph} - I_{D1} - I_{Rp} \quad (1)$$

The photo current is proportional to the incident flux and to the diffusion lengths of the carriers.

$$I = q.g(L_h - L_P) \quad (2)$$

The current in the parallel resistor has for expression:

$$I_{RP} = \frac{V_{D1}}{R_p} \quad (3)$$

And the current in diode has for expression:

$$I_{D1} = I_0(e^{\frac{qV_{D1}}{AKT}} - 1) \quad (4)$$

A, T, K, q and I_0 are respectively, idealistic factor of the cell (which depends on the recombination mechanisms of the space charge zone), temperature of the environment, Boltzmann constant ($138*10^{-23}$ J/K), The electron charge and the reverse saturation current of the diode.

By putting (3), (4) in (1), we have:

$$I = I_{ph} - I_0(e^{\frac{qV_{D1}}{AKT}} - 1) - \frac{V_{D1}}{R_p} \quad (5)$$

Where $V_{D1} = V + R_S I$ (6)

By doing (6) in (5), we have:

$$I = I_{ph} - I_0(e^{\frac{qV_{D1}}{AKT}} - 1) - \frac{(V + R_S I)}{R_p} \quad (7)$$

And in addition,

$$I_{Ph} = (I_{CC} + K_i(T - 298.15))\frac{G}{1000} \quad (8)$$

Where: I_{CC} , K_{CC} and G represent respectively the short-circuit current of the cell, the short-circuit temperature coefficient and solar irradiation.

2.1.2 Modeling of the photovoltaic module

A photovoltaic panel module is made up of several cells. Let Np be the parallel cell number of the module and Ns the serial cell number (Np=98 and Ns=12).

Then we can rewrite equation (7) by introducing the number of cells into it as follows[2]:

$$I = N_P I_{ph} - I_0(e^{\frac{q(\frac{V}{N_S} + \frac{R_S I}{N_P})}{AKT}} - 1) - (\frac{\frac{N_P V}{N_S} + R_S I}{R_P}) \quad (9)$$

Equations (8) and (9), allow us to plot the I-V and P-V characteristics of figures 3 and 4 below at a solar irradiation varying from 400W / m^2 to 1000W / m^2 at an ambient temperature of 30^0C for a solar power plant of 250kW.

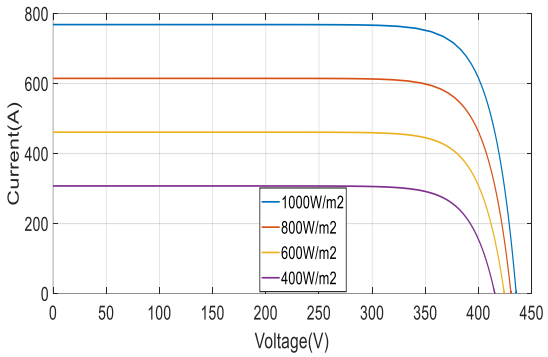

Fig.3. I-V characteristic curve

We observe in Figure 3 that the increase in illumination leads to an increase in current.

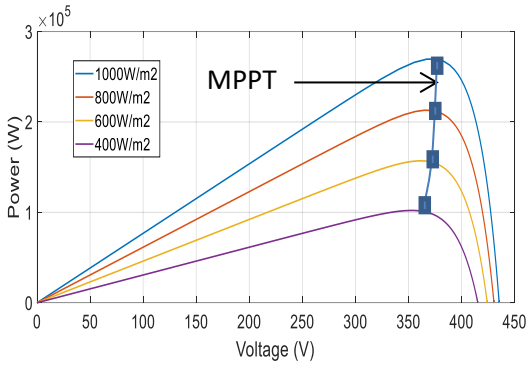

Fig.4. P-V characteristic curve

It can be seen in figure 4 that the power and the voltage increase with the lighting. And there are maximum power points that we can extract anytime by MPPT algorithm.

2.2. Modeling of the Boost Chopper With the Load

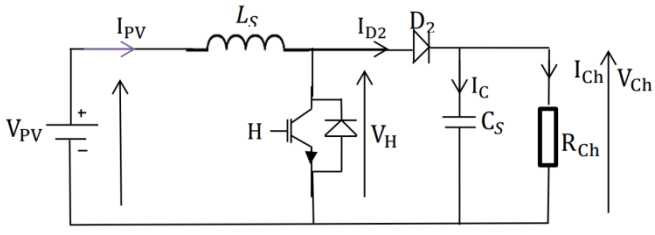

Fig.5. Boost chopper diagram

Figure 5 above shows the Boost parallel chopper. Its modeling consists in determining the relationships between the voltages, powers and currents as a function of the duty cycle D.

Expressions of the voltages, powers and currents can be developed as follows [10]:

We can therefore deduce the following power expression:

$$P_{ch} = V_{ch} I_{ch} = \frac{V_{ch}^2}{(1-D)^2 . R_{ch}} \quad (10)$$

We can see in equation (10) that an increase in the duty cycle implies a decrease in the voltage of the PV, and a decrease in the duty cycle increases the voltage of the PV. And also in equation (11) that any variation in the duty cycle has a direct impact on horsepower.

The fuzzy regulator that we will develop later will allow us to determine this duty cycle and the Duty Cycle Modulator will allow us to convert this duty cycle into control pulses, allowing us to control the electronic switches.

2.3. Modeling of fuzzy MPPT-DCM

The main idea is to combine the disturbance and observation method in a fuzzy-MRC controller taking into account the direction of variation of the disturbances. The P-V characteristic of the photovoltaic panel being concave

(figure 4), we can deduce that if a positive increase in the voltage V creates an increase in the power P, this means that the operating point is to the left of the MPP ($\frac{dP}{dV} > 0$). Moreover, if its derivative is less than zero ($\frac{d^2P}{dV^2} < 0$), that is, we are approaching the PPM, so we continue in that direction. So $\frac{d^2P}{dV^2} > 0$, we are far from the PPM, so we must increase the voltage V to reach the PPM. On the other hand, if the power decreases during an increase in voltage, this means that the operating point is to the right of the MPP ($\frac{dP}{dV} < 0$). So the derivative $\frac{d^2P}{dV^2} > 0$ that is, we are approaching the PPM, so we continue in this direction. So $\frac{d^2P}{dV^2} < 0$ we are far from the PPM, then we must decrease the voltage V to reach the PPM. If we are close to the MPP ($\frac{dP}{dV} \approx 0$), the disturbance is stopped [2]. These decreases and increases in voltage are made by varying the duty cycle. This algorithm is given in figure 6 below.

$$\begin{cases} V_{ch} = \dfrac{V_{PV}}{1-D} \\ I_{ch} = \dfrac{V_{ch}}{R_{ch}} = \dfrac{V_{PV}}{(1-D).R_{ch}} \end{cases} \quad (11)$$

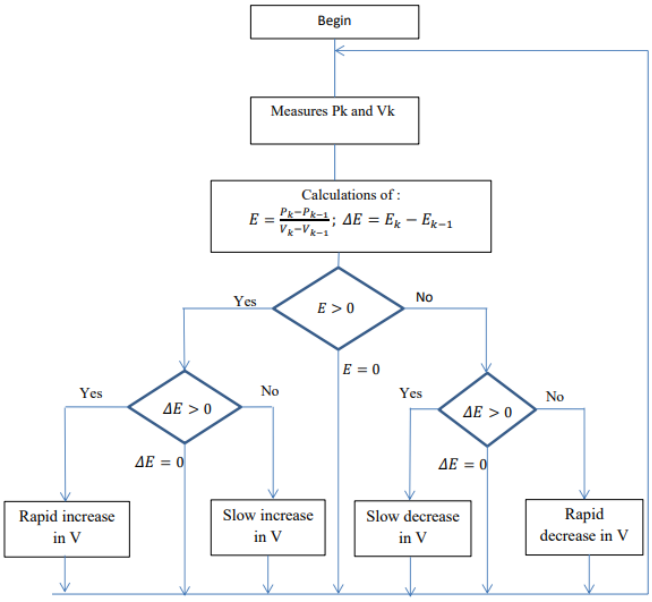

Fig.6. The MPPT Algorithm

2.3.1 Modelling of the fuzzy controller

The modelling of the fuzzy controller can be summed up in three stages: fuzzification, inference and defuzzification. The basic structure of this logic is given in figure7 below.

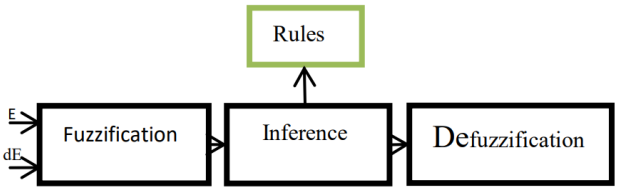

Fig.7. Basic structure of fuzzy logic.

Fuzzification: it consists of converting the real input variables into a fuzzy set. We have two entries in our case (E and dE). The E represents the first derivative of the power and the dE the second derivative. The equations for these inputs are as follows:

$$E = \frac{dP}{dV} = \frac{P_k - P_{k-1}}{V_k - V_{k-1}} \quad (12)$$

$$dE = \frac{d^2P}{dV^2} = E_k - E_{k-1} \quad (13)$$

We attribute to them the following linguistic variables: Very Negative (TN), Negative(N), Zero (Z), Positive (P) and Very Positive (TP). Their membership functions are shown in figure 8 below.

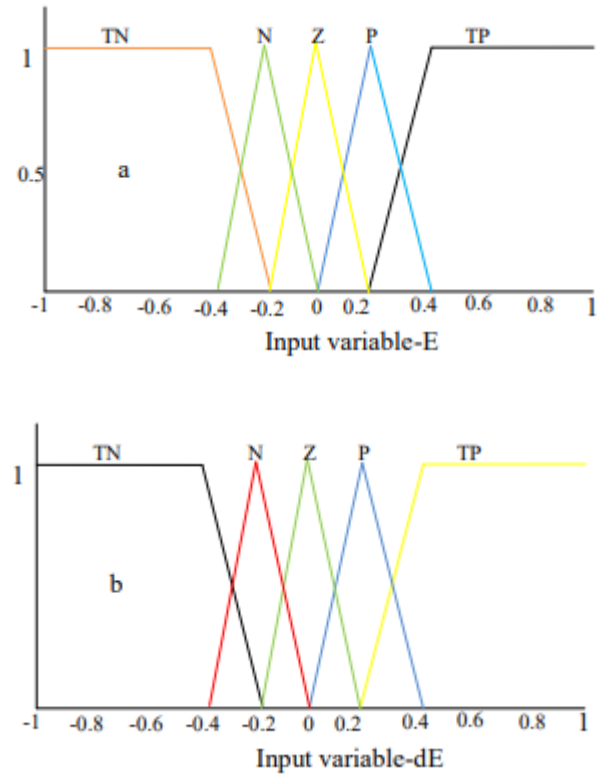

Fig.8. Membership functions of inputs.

Inference: the input variables are compared to predefined

sets (rules) to determine the appropriate response (output). In our case, we have chosen the fuzzy rules of the Takagi-Sugeno type. All this is indicated in the following Table1

Table1. ΔD Variation rules

$\frac{dP}{dV}$	$\frac{d^2P}{dV^2}$	TN(%)	N(%)	Z(%)	P(%)	TP(%)
	TN(%)	+2	+2	+1	0	0
	N(%)	+2	+1	+1	0	0
	Z(%)	0	0	0	0	0
	P(%)	0	0	-1	-1	-2
	TP(%)	0	0	-1	-2	-2

Defuzzification: this is the reverse of Fuzzification, it consists of converting the fuzzy output subsets to real values. This real value of duty cycle will be converted into control pulses by the DCM, this modulator is developed in the following paragraphs.

2.3.2 Modelling of the DCM and PWM modulator

a. DCM Modulator

The DCM is a relaxation oscillator whose principle is taken from that of tantalum vase. This modulator is under deep studies since 2005 [14]. Today, it is totally master in term of modelling and optimisation of its intrinsic parameters that makes it operate in linear mode. Basically, it based on the use of a negative resistor and it structure presents a double feedback as shown in figure 9.

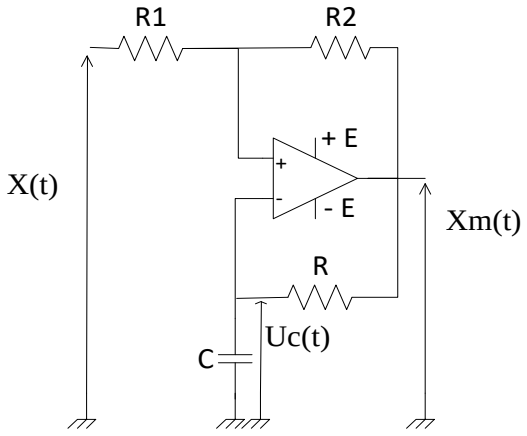

Fig.9.Diagram of the DCM

In our system, x(t) is the input signal of the modulator and represent the output signal of the fuzzy controller. $x_m(t)$ the modulator output signal to be use to drive the chopper.

Equations

For the sec of better understanding, it is recalled below the equations that governs the behaviour of the DCM modulator.

Expressions of the voltage at the inputs of the OPAM can be developed as follows [15]-[16] :

$$\begin{cases} e^{+} = \dfrac{\dfrac{x}{R_1}+\dfrac{x_m}{R_2}}{\dfrac{1}{R_1}+\dfrac{1}{R_2}} = \dfrac{R_2 x + R_1 x_m}{R_1 + R_2} \\ e^{-} = U_C \end{cases} \quad (14)$$

The dynamic behaviour of the modulator is governed by equations (15).

$$\begin{cases} e^{+}(t) = \beta x(t) + \alpha x_m(t) \\ \varepsilon(t) = e^{+} - e^{-} \\ x_m(t) = E\,\mathrm{sign}(\varepsilon(t)) \\ \dfrac{du_c(t)}{dt} = \dfrac{1}{R_1} u_c(t) + \dfrac{1}{\tau} x_m(t) \end{cases} \quad (15)$$

Where the intrinsic parameters of the modulator:

$$\alpha = \frac{R_1}{R_1 + R_2},\ \beta = \frac{R_2}{R_1 + R_2} \text{ and } \tau = RC \quad (16)$$

The DCM is therefore characterized by:

His period $T(x,\alpha)_m$.

$$T(x,\alpha)_m = \tau \log\left[\frac{(\beta x)^2 - ((1-\alpha)E)^2}{(\beta x)^2 - ((\alpha-1)E)^2}\right] \quad (17)$$

And its duty cycle R_m

$$R_m = \frac{T_{on}(x,\alpha)}{T(x,\alpha)_m} \quad (18)$$

$$R_m = \frac{\log\left[\dfrac{(1-\alpha)x - ((1+\alpha)E}{(1-\alpha)x - ((\alpha-1)E}\right]}{\log\left[\dfrac{(\beta x) - ((1-\alpha)E)}{(\beta x) - ((\alpha-1)E)}\right]} \quad (19)$$

It should be noted that the equation (19) is nonlinear but present a linear portion as we can see in Figure 9. This linear portion can be enlarged by optimizing the choice of α and β values [18]. This led to a linear approximation of equation (19) given by equation (20). It is demonstrated that both equations are almost identical [1].

$$R_m = \frac{\alpha x}{E(1+\alpha)\log(\dfrac{1+\alpha}{1-\alpha})} + \frac{1}{2} \quad (20)$$

Figure 10 shows the variations of R_m and R_m as a function of the input voltage x(t). With = 0.6 and E = 15V.

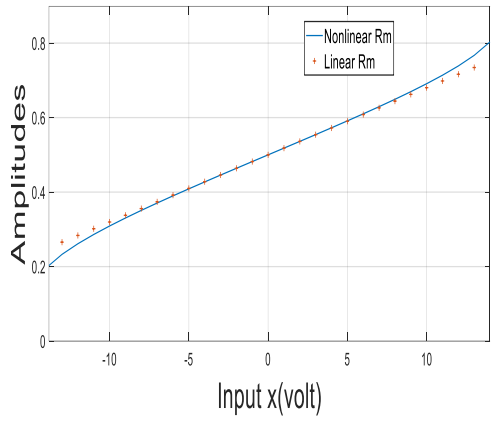

Fig. 10: Variation of the duty cycle depending on the input voltage

Oscillation frequency $F(x,\alpha)_m$

$$F(x,\alpha)_m = \frac{1}{RC.\log\left[\frac{(\beta x)^2-((1-\alpha)E)^2}{(\beta x)^2-((\alpha-1)E)^2}\right]} \quad (21)$$

For x (t) = 0, we have:

$$F(0,\alpha)_m = \frac{1}{2RC.\log\left[\frac{(1-\alpha)}{(\alpha-1)}\right]} \quad (22)$$

Figures 11 and 12 show the frequency and pulse variations according to the input signal. With

$R_1 = R = 10k\Omega, R_2 = 8.2k\Omega, C = 0.8096nF$

$E = 15V$

And x (t) varies between -10V to 10V

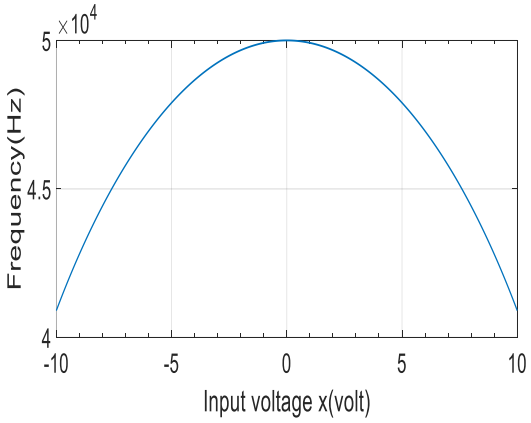

Fig.11.Curve of changes in frequencydepending on the input voltage

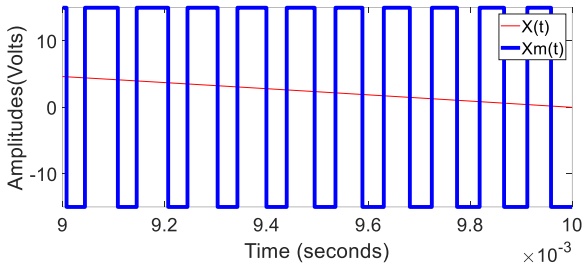

Fig.12.variation of output pulses (Xm(t)) as a function of input signal (X(t)).

It can be seen in figure 12 that the frequency, the duty cycle therefore the pulses of the DCM, vary with the input signal x (t). This will allow us to control the chopper

b. PWM Modulator

The scheme of a PWM signal generator is shown in figure 13. It consists to a triangular signal generator which produces a carrier and an inverting comparator whose output switches as a function of the difference between the carrier and the control signal x [19]-[20].

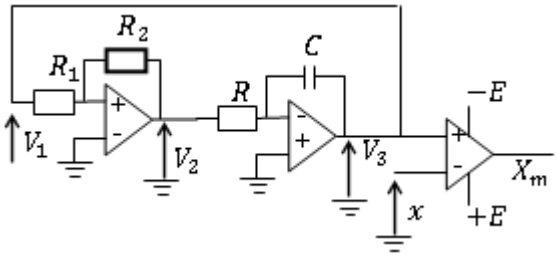

Fig.13.Diagram of the PWM

This modulator is the most used to control converters in order to extract the maximum power from renewable energies [21]-[22]. The modeling equations of this modulator are developed below.

Equations

For the sec of better understanding, it is recalled below the equations that governs the behaviour of the PWM modulator [23]-[24].

The PWM is therefore characterized by:

His period $T(x)_m$.

$$T(x)_m = 4R_1RC / R_2 \quad (23)$$

And its duty cycle R_m

$$R_m = \frac{T_{on}(x)}{T(x)_m} \quad (24)$$

$$R_m = \frac{1}{2}[1-\frac{x}{E}.\frac{R_2}{R_1}] \quad (25)$$

Oscillation frequency $F(x)_m$

$$F_m = R2/4R1RC \quad (26)$$

For F_m =50kHz, we have:

$$R_1 = R = 10k\Omega, R_2 = 8.2k\Omega, C = 1.025nF$$

$$E = 15V$$

3. Simulations and Analysis of Results

Virtual simulations are performed on the Matlab / Simulink environment to compare the MPPT-Fuzzy-PWM and MPPT-Fuzzy-DCM command. To compare these two commands, you must define the comparison criteria. In our case, we are going to make the comparison on the precision and the speed of convergence at the same modulation frequency (50 kHz), and having the same fuzzy controller. In addition, the signal coming from the fuzzy controller being normalized from 0 to 1, and the PWM modulator placed directly after this controller also being normalized from 0 to 1 in Matlab / Simulink, these two blocks can be directly connected without amplification. On the other hand, the DCM not being standardized in this software, we use a gain of 15, in order to have an input voltage of the DCM between 0 and 15, corresponding to its operating range.

3.1. Simulation Diagram

The following figure 14 represents the eastern simulation diagram of our system

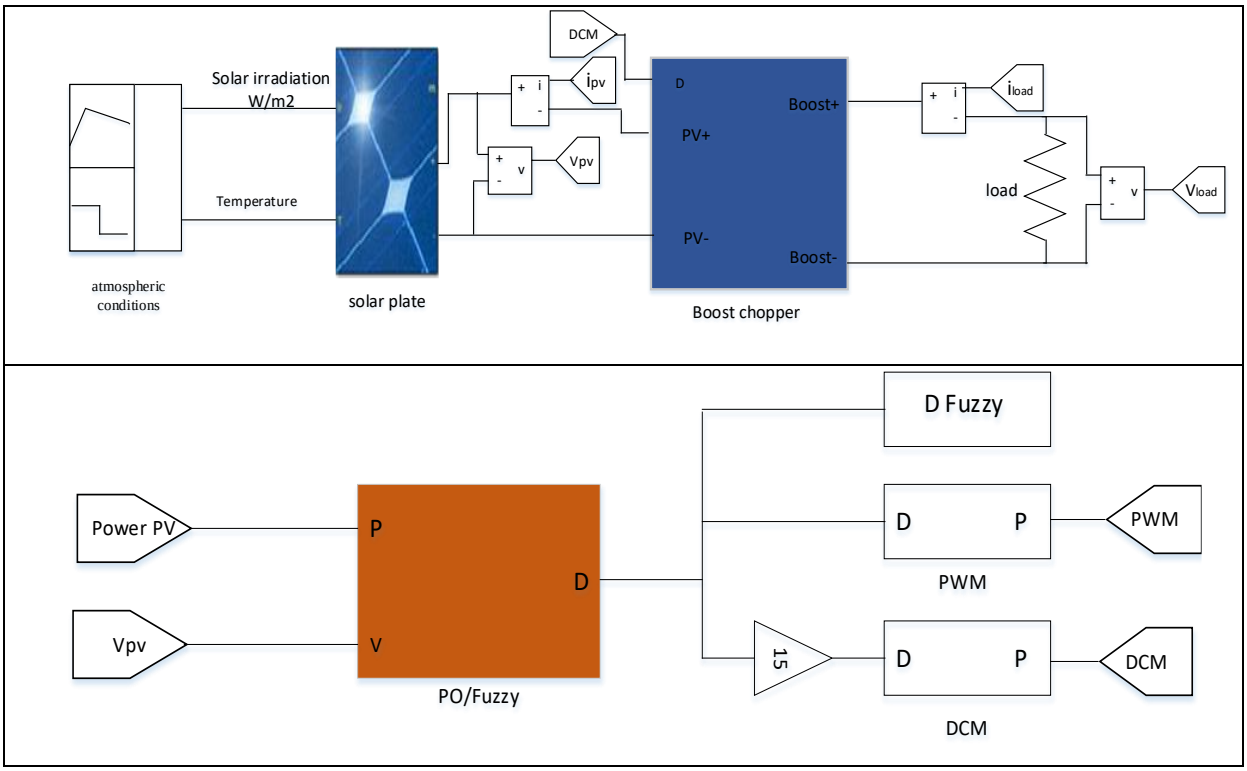

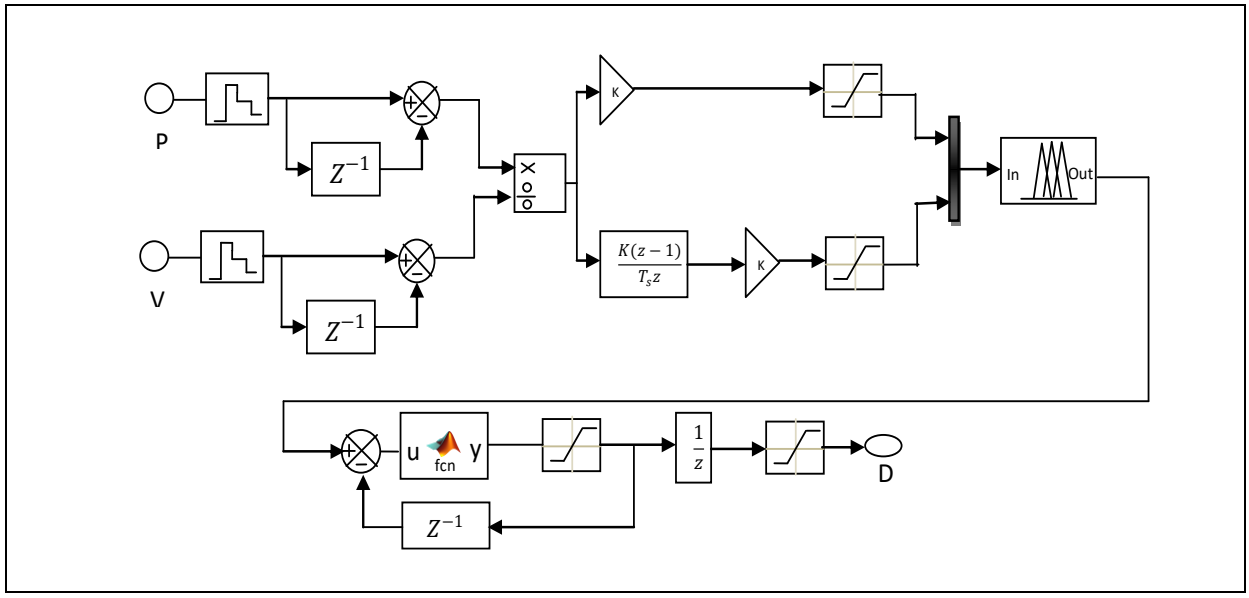

Fig.14. Simulation diagram

3.2. Simulation results

Data: G= [1000, 800], T30^{0}C, P=250 kW and F=50 kHz

The following figure 15 represents the results of the simulations

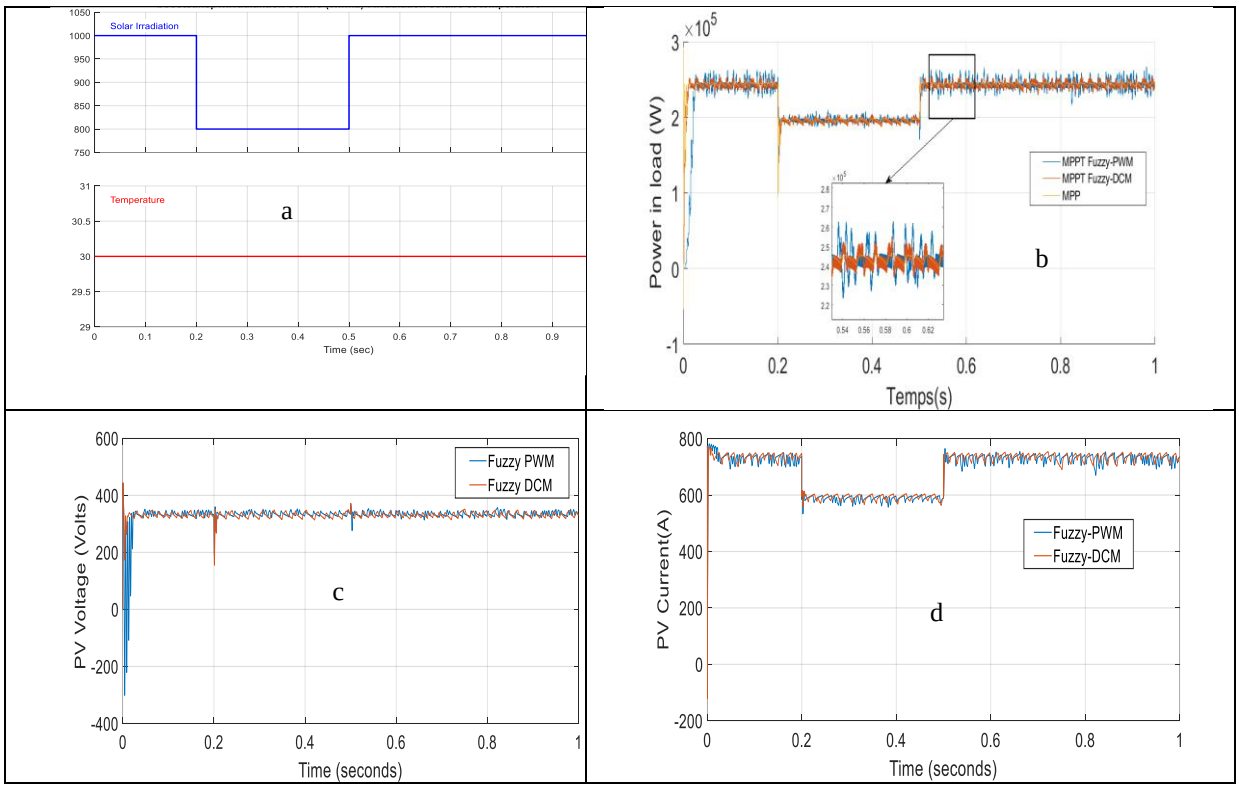

Fig.15.Power, voltage and current curves of the MPPT Fuzzy-PWM and DCM

3.3. Results analysis

3.3.1. Power analysis.

a. For irradiation of 1000 W/m^2

For the solar irradiation of 1000W/m^2, the MPPT Fuzzy-PWM and MPPT Fuzzy-DCM curves of figure 15-b, give us the values of the following table 2.

We find that the MPPT Fuzzy-PWM command has a response time of 0.02652 s, while that of the MPPT Fuzzy-DCM command is 0.01317 s, so the MPPT Fuzzy-DCM command converges faster (i.e. 2.013 times more) than that of MPPT Fuzzy-PWM. In addition, we observe the power oscillations ranging from 216.4 kW up to 266.6 kW for the MPPT Fuzzy-PWM, and going from 231.1 kW up to 252.3 kW for the MPPT Fuzzy-DCM.

Table2. Comparison table of the two controls for an irradiation of 1000 W/m^2

	MPPT Fuzzy-PWM	**MPPT Fuzzy-DCM**
Response time (s)	0.02652	0.01317
Maximum power (kW)	266.6	252.3
Minimum power (kW)	216.4	231.1
ΔP (kW)	0.502	0.212

Therefore, the MPPT Fuzzy-DCM command produces less power oscillation (i.e. 2.36 times less) than the MPPT Fuzzy-PWM.

b. For Irradiation of 800 W/m^2

As previously, the MPPT Fuzzy-PWM and MPPT Fuzzy-DCM curves in figure 15-b, for an irradiation of 800 W / m^2, give us the values in the following table3:

Table3. Comparison table of the two controls for an irradiation of 800 W / m^2

	MPPT Fuzzy-PWM	**MPPT Fuzzy-DCM**
Maximum power (kW)	**210**	**202.3**
Minimum power (kW)	**186.3**	**188.1**
ΔP (kW)	**0.237**	**0.142**

We find that the Fuzzy-PWM MPPT drives power oscillations ranging from 186.3 kW up to 210 kW and ranging from 188.1Kw up to 202.3 kW for the Fuzzy-DCM MPPT. Therefore, the MPPT Fuzzy-DCM control produces less power oscillation (i.e. 1,669 times less) than the MPPT Fuzzy-PWM.

3.3.2. Voltage and current analysis.

a. For irradiation of 1000W / m^2

For solar irradiation of 1000W / m^2, the curves of variation of voltages and currents of figures 15-c and 15-d, give us the values of the following table4:

Table4. Comparison table of the two commands in voltages and in currents.

V_{PV}**(V)**	I_{PV}**(A)**		
0.0231	**0.004**	**Fuzzy-PWM**	**Response time(s)**
0.0138	**0.004**	**Fuzzy-DCM**	
350.9	**750**	**Fuzzy-PWM**	**Maximum value**
348.5	**749**	**Fuzzy-DCM**	
319	**700.9**	**Fuzzy-PWM**	**Minimum value**
319.9	**704.2**	**Fuzzy-DCM**	

Table4 shows that the oscillations of voltages and currents are reduced for the fuzzy-DCM strategy compared to the fuzzy-PWM strategy. In addition, the response time of the fuzzy-DCM strategy is reduced compared to the fuzzy-PWM strategy.

b. For irradiation of 800W / m^2

For solar irradiation of 800W / m^2, the curves of variation of voltages and currents of figures 15-c and 15-d, give us the values of the following table5:

Table5. Comparison table of the two commands in voltages and in currents.

V_{PV}**(V)**	I_{PV}**(A)**		
352.48	**602.11**	**Fuzzy-PWM**	**Maximum value**
348.53	**604.08**	**Fuzzy-DCM**	
319.32	**556.49**	**Fuzzy-PWM**	**Minimum value**
313.82	**566.07**	**Fuzzy-DCM**	

According to the table5, except for the voltage V_{pv}, the other oscillations voltages and currents are reduced for the fuzzy-DCM strategy compared to the fuzzy-PWM strategy.

4. Conclusion

In this work, we have described the most used MPPT algorithm for PV, which is that of perturbation and observation. Then we underlined certain limitations which sully the latter, in particular the lack of precision and speed. Next, we proposed a fuzzy MPPT-DCM to overcome these limitations. Finally, a simulation and analysis of the results of the MPPT Fuzzy -PWM and the MPPT Fuzzy-DCM were carried out for a 250KW solar power plant. It turns out that our

fuzzy MPPT-DCM strategy is more accurate (2.36 times) and faster (2.013 times) than the fuzzy MPPT-PWM strategy.

In the future, we are first interested in improving these results by trying Neuro-DCM (N-DCM) and then Neuro-Fuzzy-DCM (NF-DCM) controllers. Then we will implement this strategy in a real system. Then we will broaden its fields of application, in particular on wind and tidal turbines. Finally, an experimental study to validate the theoretical results could be considered later.

References

[1] A. O. Biyobo, L. N. Nneme, J. Mbihi, F. Pauné, and B. L. Moffo,"Étude expérimentale d'un nouveau modèle d'onduleur solaire monophasé à modulation en rapport cyclique", Afrique SCIENCE, vol. 16, no 2, p. 118-131, 2020.

[2] H. Essakhi, S. Farhat, M. Mediouni, and Y. Dbaghi, "Improving the dynamic performances of an MPPT controller for a Photovoltaic system using fuzzy logic", E3S Web Conf., vol. 229, p. 01013, 2021, doi: 10.1051/e3sconf/202122901013.

[3] K. Behihet,and H. Attoui, "Backstepping Terminal Sliding Mode MPPT Controller for Photovoltaic Systems", Engineering, Technology & Applied Science Research, vol. 11, no 2, Art. no 2, April. 2021, doi: 10.48084/etasr.4101.

[4] H. Doubabi, I. Salhi, M. Chennani, and N. Essounbouli, "High Performance MPPT based on TS Fuzzy–integral back stepping control for PV system under rapid varying irradiance—Experimental validation", ISA Transactions, vol. 118, p. 247-259, Décember 2021, doi: 10.1016/j.isatra.2021.02.004.

[5] A. I. Nusaif, and A. L. Mahmood, "MPPT Algorithms (PSO, FA, and MFA) for PV System Under Partial Shading Condition, Case Study: BTS in Algazalia, Baghdad", International Journal of Smart Grid - ijSmartGrid, vol. 4, no 3, Art. no 3, sept. 2020.

[6] A. J. H. A. Gizi, "PLC Fuzzy PID Controller of MPPT of Solar Energy Converter", WSEAS Transactions on Systems and Control, vol. 16, p. 1-20, 2021, doi: 10.37394/23203.2021.16.1.

[7] M. Sabitha, and D. Kumar, "Fuzzy Based MPPT Controller For Solar Photovoltaic Systems", International Journal of Advanced Research in Science, Communication and Technology, p. 359-370, May 2021, doi: 10.48175/IJARSCT-1095.

[8] F. Oudiai, K. Lagha-Menouer, A. Hadj Arab,and Z. Rachid, "Commande MPPT et Contrôle d'un Système Photovoltaïque par Incrément de la Conductance", the 2nd International Seminar on Fossil, New and RenewableEnergy, November. 13-14, 2019, Boumerdes, Algeria.

[9] Y. Furukawa, H. Tomura, T. Suetsugu, and F. Kurokawa, "Variable Feedback Gain DC-DC Converer Tracing Output Voltage Fluctuation for Renewable Energy System", in 2019 8th International Conference on Renewable Energy Research and Applications (ICRERA), November. 2019, p. 916-921. doi: 10.1109/ICRERA47325.2019.8996540.

[10] S. Marhraoui, A. Abbou, N. El Hichami, S. E. Rhaili, and M. R. Tur, "Grid-Connected PV Using Sliding Mode Based on Incremental Conductance MPPT and VSC", in 2019 8th International Conference on Renewable Energy Research and Applications (ICRERA), November. 2019, p. 516-520. doi: 10.1109/ICRERA47325.2019.8996621

[11] M. N. Ali, K. Mahmoud, M. Lehtonen, and M. M. F. Darwish, "Promising MPPT Methods Combining Metaheuristic, Fuzzy-Logic and ANN Techniques for Grid-Connected Photovoltaic", Sensors (Basel), vol. 21, no 4, p. 1244, February. 2021, doi: 10.3390/s21041244.

[12] A. O. Biyobo, L. N. Nneme, and J. Mbihi,"A novel sine duty-cycle modulation control scheme for photovoltaic single-phase power inverters", WSEAS Transactions on circuits and Systems, vol. 17, p. 107-113, 2018.

[13] P. O. Etouke, L. N. Nneme, and J. Mbihi, "An Optimal Control Scheme for a Class of Duty-Cycle Modulation Buck Choppers: Analog Design and Virtual Simulation", Journal of Electrical Engineering, Electronics, Control and Computer Science, vol. 6, no 1, p. 13-20, 2020.

[14] J. Mbihi, B. Ndjali, and M. Mbouenda, "Modelling And Simulation of A Class of Duty-Cycle Modulators For Industrial Instrumentation", Iranian Journal of Electrical and Computer Engineering (IJECE), vol. 4, no. 2, pp. 121-128, 2005, iran, issn: 1682-0053.

[15] G. Sonfack, J. Mbihi, and B. L. Moffo, "Optimal duty-cycle modulation scheme for analog-to-digital conversion systems", International Journal of Electronics and communication engineering,\copyright World Academic of Science, Engineering and Technology, vol. 11, no 3, p. 354-360, 2017, doi: doi.org/10.5281/zenodo.1315523.

[16] S. G. Béatrice, and M. Jean, "FPGA-Based Analog-to-Digital Conversion via Optimal Duty-Cycle Modulation", Electrical and Electronic Engineering, vol. 8, no 2, p. 29-36, 2018, doi: 10.5923/j.eee.20180802.01.

[17] S. F. Jaber and A. M. Shakir, "Design and Simulation of a Boost-Microinverter for Optimized Photovoltaic System Performance", International Journal of Smart Grid - ijSmartGrid, vol. 5, no 2, Art. no 2, june 2021.

[18] L. N. Nneme, and J. Mbihi, "Virtual Simultion and Comparison of Sine Pulse Width and Sine Duty Cycle

modulation Drivers or Single Phase Power Inverters", Journal of Electrical Engineering, Electronics, Control and Computer Science – JEEECCS, Volume 6, Issue 21, pages 31-38, 2020.

[19] A. Belkaid, I. Colak, K. Kayisli, and R. Bayindir, "Improving PV System Performance using High Efficiency Fuzzy Logic Control ", in 2020 8th International Conference on Smart Grid (icSmartGrid), June 2020, p. 152-156. doi: 10.1109/icSmartGrid49881.2020.9144817.

[20] Y. Sanwogou, H. Hova, J. P. Yembi, H. Y. Ba, and I. Ly,"Conception d'un système solaire photovoltaïque pour alimenter le laboratoire de physique de l'Université de Kara, Togo", Afrique SCIENCE, vol. 15, no 5, p. 238-251, 2019.

[21] A. Sandali, and A. Cheriti, "Maximum Power Characteristic Tracking: Definition and Adaptation to Various Power Electronics Converters", International Journal on Energy Conversion (IRECON), vol. 7, p. 38, January. 2019, doi: 10.15866/irecon.v7i1.16160.

[22] M. Qasim, and V. Velkin, "Maximum Power Point Tracking Techniques for Micro-Grid Hybrid Wind and Solar Energy Systems - a Review", International Journal on Energy Conversion (IRECON), vol. 8, p. 223, nov. 2020, doi: 10.15866/irecon.v8i6.19502.

[23] A. Rachid, R. Chenni, and F. Kerrour, "An Accurate Photovoltaic Emulator Based on Two Closed-Loop Control Systems Including Partial Shading Conditions", International Journal on Energy Conversion (IRECON), vol. 7, no 4, Art. no 4, July. 2019, doi: 10.15866/irecon.v7i4.16815.

[24] G. M. Ngaleu, C. H. Kom, A. T. Yeremou, S. Eke, and A. Nanfak, "Design of New Duty-Cycle Modulator Structures for Industrials Applications, an Alternative to Pulse-Width Modulation", EJEE, vol. 23, no 2, p. 103-111, April. 2021, doi: 10.18280/ejee.230203.